

Recent Results from the Experimental Nuclear Structure Program at iThemba LABS

J. J. Lawrie¹, R. Bark¹, N. T. Botha^{1,2}, O. Burda³, J. Carter⁴, R. W. Fearick², S. V. Förtsch¹, C. Fransen⁵, H. Fujita^{1,4}, M. Kuhar³, E. A. Lawrie¹, A. Lenhardt³, R. Lindsay⁶, M. Lipoglavšek^{1,7}, S. M. Maliage^{1,6}, B. M. Msezane^{1,8}, L. J. Mudau^{1,6}, S. M. Mullins¹, P. Mutshena^{1,2}, O. M. Ndwandwe⁸, R. Neveling¹, S.S. Ntshangase^{1,8}, N. Pietralla^{5,9}, V. Yu. Ponomarev³, A. Richter³, N. Rowley¹⁰, O. Scholten¹¹, J. F. Sharpey-Schafer¹, E. Sideras-Haddad⁴, G. Sletten¹², F. D. Smit¹, C. Theron¹, P. von Neumann-Cose³, and J. Wambach³

¹ iThemba LABS, PO Box 722, Somerset West 7129, South Africa

² Physics Department, University of Cape Town, Rondebosch 7700, South Africa

³ Institut für Kernphysik, Technische Universität Darmstadt, 64829 Darmstadt, Germany

⁴ School of Physics, University of the Witwatersrand, Johannesburg 2050, South Africa

⁵ Institut für Kernphysik, Universität zu Köln, 50397 Köln, Germany

⁶ Department of Physics, University of the Western Cape, Private Bag X17, Bellville 7535, South Africa

⁷ Josef Stefan Institute, 1000 Ljubljana, Slovenia

⁸ Department of Physics and Engineering, University of Zululand, Private Bag X1001, Kwadlangezwa 3886, South Africa

⁹ Department of Physics and Astronomy, SUNY, Stony Brook, NY 11794-3800, USA

¹⁰ Institute Interdisciplinaire Hubert Curien, Strasbourg, France

¹¹ KVI, University of Groningen, NL-9747 AA Groningen, The Netherlands

¹² Niels Bohr Institute, Copenhagen, Denmark

Abstract. The nuclear structure research program at iThemba LABS is based on the use of both light and heavy ions from the k=200 separated sector cyclotron. In a brief overview of some recent results the following experiments are presented: a) Large angle quasi-elastic scattering of ⁸⁶Kr on ²⁰⁸Pb has been studied in order to determine the fusion barrier. b) Results from a high energy-resolution proton scattering experiment at iThemba LABS were compared with similar inelastic electron scattering data obtained at the S-DALINAC, Darmstadt, to test the nature of the proposed one- and two-phonon symmetric and mixed-symmetric 2⁺ states of the nucleus ⁹⁴Mo. The combined analysis reveals the one-phonon content of the mixed-symmetry state and its isovector character as suggested by microscopic nuclear model calculations. c) In a γ -ray spectroscopy study of ¹⁹⁶Hg using the ¹⁹⁸Pt(α ,6n) reaction a new dipole band was observed and the spin and parity determined. Although dipole bands have been found in ^{192,194}Hg this new band does not have an obvious counterpart in the lighter Hg isotopes.

1 Introduction

iThemba LABS, situated near Cape Town, is South Africa's premier facility for research, training, and applications in a wide variety of disciplines that use accel-

erated particle beams, including a) particle therapy and bio-medical research, b) radioisotope production, c) nuclear physics, and d) materials science.

The nuclear physics research program makes use of light and heavy ion beams from the k=200 separated sector cyclotron (SSC). Beams from either an ECR ion source or a polarized proton ion source are accelerated in a solid pole cyclotron before being injected into the SSC. Available beams and energies range from 200 MeV protons and alpha particles to 750 MeV ^{136}Xe . The following three facilities are available for nuclear physics experiments.

The k=600 magnetic spectrometer is a kinematically corrected QDD spectrometer optimized for use with light ions. With dispersion matching an energy resolution of 30 keV can be obtained for elastic scattering of 200 MeV protons off Au. The ability to measure proton inelastic scattering at 0 degrees is being developed. The AFRODITE gamma array consists of up to 9 escape suppressed HPGe clover detectors and up to 8 four-fold segmented planar Ge detectors. The absolute efficiency at 1.33 keV is 1.6% and up to 12% at 100 keV. A 1.5 m diameter scattering chamber with two rotatable arms is available for charged particle reaction studies with Si and scintillator detector telescopes.

In the following sections results from three recent experimental studies will be presented.

2 Barrier distribution for $^{86}\text{Kr} + ^{208}\text{Pb}$

The reaction $^{86}\text{Kr} + ^{208}\text{Pb}$ has in the past been used in attempts to make a super-heavy nucleus with $Z=118$. However, thus far no evidence for compound nucleus formation, let alone evaporation residues, was forthcoming. In studying the dynamics of fusion reactions in lighter systems much has been learnt from investigations of the fusion barrier distributions [1]. In this study we investigate whether the concept of a barrier distribution is still valid for a system as heavy as $^{86}\text{Kr} + ^{208}\text{Pb}$.

For lighter systems the barrier distribution (BD), defined as $D = d^2(E\sigma)/dE^2$ can easily be obtained by measuring the evaporation residue cross-section [2]. Such a method is clearly not possible for the present case, where the total capture cross section includes fusion-evaporation, fusion-fission, quasi-fission and deep inelastic scattering cross sections. Instead, we exploit the unitarity of processes occurring at the Coulomb barrier to obtain the barrier distribution from the quasi-elastic (QE) scattering at very backward angles. In this case the distribution is given by $D = -d(\sigma_{QE}/\sigma_R)/dE$. Furthermore, since operational restrictions at iThemba LABS prevent numerous energy changes of the separated sector cyclotron, an excitation function was obtained by generating effective energies E_{eff} from different detector angles. By assuming Rutherford trajectories, each angle θ defines an angular momentum barrier for the partial waves at that angle, which can be subtracted from the incident energy to define an effective energy $E_{eff} = 2E/(1 + \text{cosec}(\theta/2))$ [3].

The experiment was performed in a 1.5 m scattering chamber, which is equipped with two arms that can rotate around the target. The one arm supported a Si surface

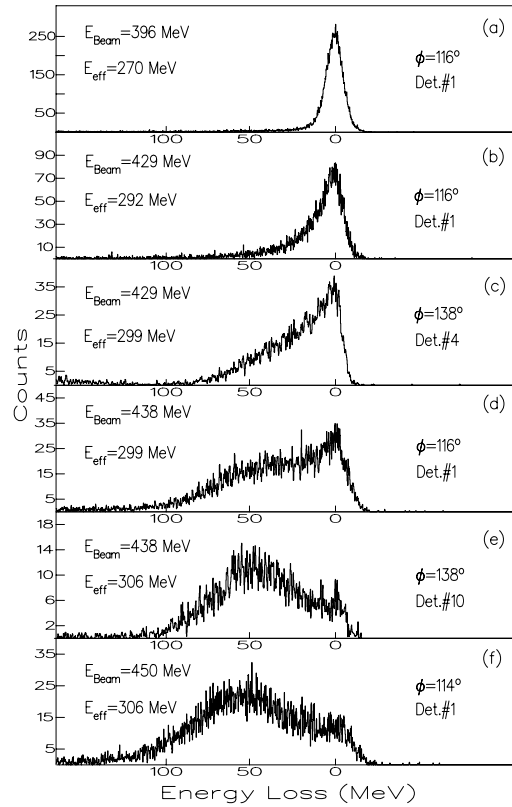


Figure 1. Representative centre of mass energy loss spectra at different beam energies and detector angles, resulting in different effective energies. The transformation to energy loss was performed assuming that a projectile-like particle is detected.

barrier detector that was positioned at 40° to monitor the beam direction detecting the elastically scattering rate. On the other arm an array of 22 photovoltaic cells, each 0.9 cm^2 in area, was mounted, with elements arranged in pairs at complementary angles in the range from $\pm 175^\circ$ to $\pm 125^\circ$ above and below the horizontal plane. This array could be positioned at various in-plane angles. Back-scattered particles were detected for five incident beam energies, ranging from well below the barrier at 396 MeV to above it at 450 MeV (lab) to yield energy spectra at corresponding effective energies from 270 to 320 MeV. Examples are given in Figure 1.

At the lowest energies a well defined symmetric peak is observed, corresponding to pure QE scattering. This peak shape defines the detector response which we assume remains fixed. At higher energies a tail of higher energy-loss events develops. We assumed that these events, that can include multi-neutron transfer taking place outside the barrier, are still as a result of reflection from the barrier. We assumed further that this component increases rapidly as the barrier is approached and reaches

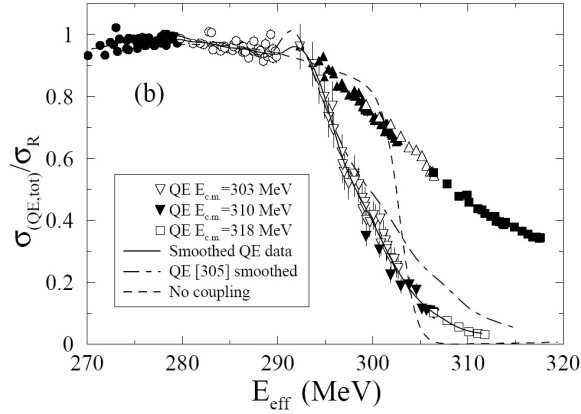


Figure 2. Total cross-section and QE cross-section normalized to σ_R and compared with no coupling and coupled channels calculation.

a maximum (of about 78% of the total area of the peak) at $E_{eff} \approx 292$ MeV after which the percentage remains constant. At higher energies a broad structure centered at an energy-loss of ≈ 50 MeV develops that increases rapidly in strength. These events are associated with deep inelastic scattering and are not included in the determination of the QE cross section. The size of the QE component was thus obtained by fitting a Gaussian to the high energy side of the QE peak, and assuming that the peak has a low energy tail that is fixed in proportion to the Gaussian part as a function of energy. Further details of this procedure are given in reference [4].

The measured cross-sections relative to Rutherford scattering, are shown as a function of E_{eff} in Figure 2. Above 290 MeV both cross sections with and without the correction for deep inelastic scattering are shown. It should be noted that in both cases the data at the same effective energy, but obtained from different incident energies, overlap. The large uncertainties preclude differentiation unless the data are first smoothed. We used a method based on the Strutinsky smoothing functions $f_k(u)exp(-u)$, where $u = (E_{eff} - E_{eff}^j)^2/\Delta^2$ and f_k is the curvature function of order $2k$. The smoothed values are given by:

$$\sigma(E_{eff}) = - \sum_j \sigma(E_{eff}^{(j)}) f_k(u) exp(-u) dE^{(j)} \quad (1)$$

The choice of the smoothing width Δ is made by plotting the standard deviation of the experimental values from the smoothed function, as a function of Δ . For $1 \leq k < 4$ a plateau region in the range $2 < \Delta < 3$ MeV is found where the standard deviation is found to be approximately independent of the choice of Δ . Therefore a smoothing width of $\Delta = 2.5$ MeV was chosen. The smoothed data is presented as a solid line in Figure 2.

The resulting barrier distribution is shown in Figure 3, where it is compared to barrier distributions calculated using the coupled channels method. A reasonable

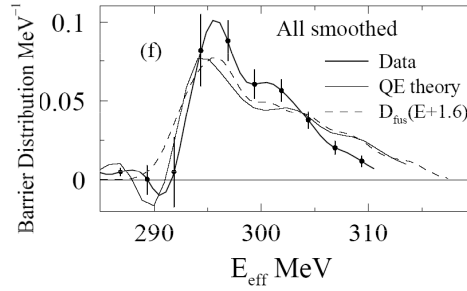


Figure 3. Experimental barrier distribution (with representative error bars), compared with theoretical barrier distribution for QE scattering and fusion (D_{fus}).

agreement is achieved with the inclusion of 5 quadrupole phonons and 3 octupole phonons, although the $3^- \rightarrow (3^-)^2$ coupling is reduced by a factor of 0.6 and the $(3^-)^2 \rightarrow (3^-)^3$ coupling by a factor $(0.6)^2$. The results show that the concept of a barrier distribution is still valid for systems as heavy as Kr on Pb. A full report has been published in [4].

3 One- and two-phonon mixed-symmetry states in ^{94}Mo in high resolution electron and proton scattering

In order to study the nature of proposed one- and two-phonon fully symmetric (FSS) and mixed symmetric (MSS) 2^+ states of the nucleus ^{94}Mo [5], a high resolution inelastic proton scattering experiment was performed at iThemba LABS. These measurements, together with those from a high resolution electron inelastic scattering experiment performed at Darmstadt TU, were compared with microscopic calculations.

The high resolution (p, p') measurements at an incident proton energy of 200 MeV were performed using the k=600 magnetic spectrometer, and techniques similar to those described in [6] except for the additional use of the faint beam method [7], which facilitated the optimization of dispersion-matched conditions. Data were acquired at scattering angles from 6° to 27° . Typically the energy resolution was ≈ 35 keV (FWHM). The very good energy resolution was essential to extract accurate cross sections for weak transitions.

In Figure 4 the measured (p, p') and (e, e') cross sections for the one- and two-phonon candidates that were identified in reference [5], are compared with the re-

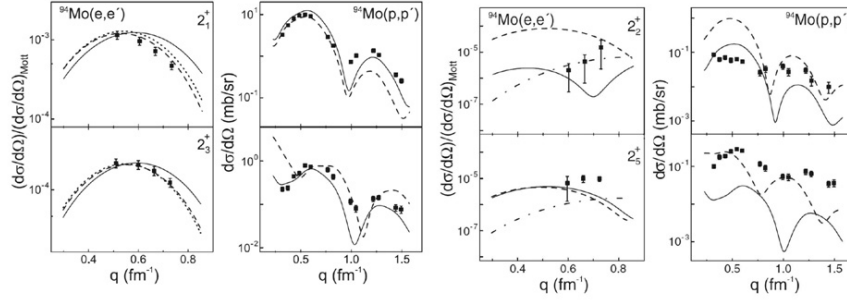


Figure 4. Momentum transfer dependence of the excitation of the one-phonon (l.h.s.) and two-phonon (r.h.s.) FSS (top) and MSS (bottom) in ^{94}Mo observed in electron and proton scatterings, respectively.

sults of microscopic quasiparticle phonon model (QPM), shell model (SM), and IBM-2 calculations. For details of the theoretical calculations, see reference [8].

The left hand side of Figure 4 presents the results for the transitions populating the one-phonon FSS (2_1^+) and MSS (2_3^+) in ^{94}Mo . Taking into account an overall uncertainty of about 25% due to the choice of the effective interaction [9], the QPM accounts well for the proton scattering results. The SM results are poorly matched to the proton scattering data for higher momentum transfers, where correlations outside the valence space become important.

The right hand side of Figure 4 shows the results of the two-phonon FSS (2_2^+) and MSS (2_5^+). Here, the SM fails for the (e, e') results. The QPM with larger model space provides cross sections of the correct magnitude for the two-phonon symmetric state, although it predicts a pronounced minimum at a momentum transfer $q \approx 0.72 \text{ fm}^{-1}$ due to an interference of the one- and two-phonon components; this minimum is not observed in the data. However, simplified QPM calculations considering the basic one- and two-phonon states allow a good description to be achieved. This indicates the symmetric two-phonon state to be very pure. For the mixed-symmetry candidate, the full QPM results are somewhat small but account roughly for the momentum transfer dependence. As can be seen on the right hand side of Figure 4, both SM and QPM results deviate from the (p, p') experimental data. A possible explanation is the neglect of two step processes in the reaction mechanism.

In order to estimate the two step processes, a coupled channel analysis was performed with the code CHUCK3 [10]. The left hand side of Figure 5 indicates the coupling schemes taken into account for the two-phonon FSS and MSS, respectively. The CHUCK3 results for the two-phonon states are displayed on the right hand side of Figure 5.

The best description of the 2_2^+ state is achieved by a vanishing one step amplitude (the coupling strength $\beta = 0$), i.e. the conclusion drawn from the electron scattering results that it has an almost pure two-phonon nature, is confirmed. For the mixed-symmetry state, the best description is achieved when $\beta = 0.2$. Thus, the

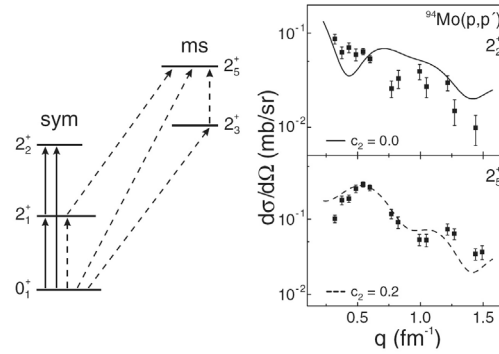


Figure 5. Coupled-channel analysis for the excitation of the two-phonon FSS and MSS in the $^{94}\text{Mo}(p, p')$ experiment.

addition of two-step contributions to the (p, p') cross sections provides a picture that is fully consistent with the data obtained from both experimental probes.

The combination of electromagnetic and hadronic scatterings opens a new experimental avenue for future investigations of mixed symmetry states. One obvious application would be the study of ^{92}Zr , where a description in terms of symmetric and mixed-symmetric states seems to fail [11, 12].

4 Dipole Bands in ^{196}Hg

Medium-mass mercury nuclei are weakly oblate in their ground state and up to high spins. In previous studies dipole bands were observed in a number of even Hg isotopes, including ^{196}Hg where one dipole band was found by Cederwall et al [13]. In a recent experiment at iThemba LABS we observed a second dipole band in ^{196}Hg and could make an unambiguous spin and parity assignment from DCO and polarization measurements.

The experiment was performed using the AFRODITE array that, at the time, consisted of 7 suppressed clover detectors and 7 segmented planar Ge detectors. ^{196}Hg was populated in the $^{194}\text{Pt}(\alpha, 6n)$ reaction at 65 MeV. Since the initial purpose of the experiment was to calibrate the AFRODITE array for lifetime measurements with the Recoil Shadow Anisotropy Method (RSAM) as reported in [14], we used a thin (0.2 mg/cm^2) target and employed 6 of the 7 clover detectors at 90° . A smaller set of data was also obtained with clover detectors symmetrically arranged at 45° , 90° and 135° which could be used for DCO measurements.

The decay scheme obtained from a study of $\gamma - \gamma$ coincidences generally confirms and extends the level scheme reported by Mehta et al. [15]. We also observed the dipole band (Figure 6) reported by Cederwall et al. [13], here labelled DB1, and also found decay out of this band by a 1406 keV transition to the 21^- state at 5039 keV (band ABCE). However we could not determine the multipolarity of this tran-

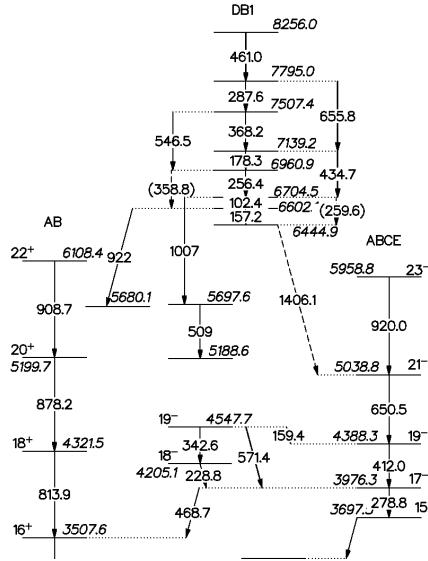


Figure 6. A partial level scheme of ^{196}Hg indicating the dipole band DB1 as obtained from the present study.

sition nor could we exclude additional levels in this decay chain, and thus could not assign spin or parity to the band. Other decay paths out of this band, e.g. the decay via the 1005 and 509 keV gammas, that feed the 19^- level at 4548 keV through unobserved transitions, are also indicated.

In addition we observed a second dipole band (DB2), shown in the partial level scheme of Figure 7 that extends both above and below previously observed levels at 5351, 5617 and 5860 keV [15]. DCO and polarization measurements on the 266 and 243 keV transitions confirmed their M1 nature. Similarly the 821, 963, and 1147 transitions that depopulate the band towards the ABCE negative parity band are measured to be E1 transitions, thus fixing the spin and parity of the band.

We can compare qualitative features of DB2 with dipole bands observed in $^{192,194}\text{Hg}$. Two dipole bands are observed in ^{194}Hg [16]. The first ("structure 1" in reference [16]) is at relatively high excitation and spin ($E_{ex} = 9600$ keV and $I = 31\hbar$) and decays to the positive parity AB and ABCD bands. No counterpart of this band is observed in the present work. The second at 6790 keV ("structure 2" in reference [16]) probably has a bandhead spin of 23 or 24 but the parity is not assigned. The decay out of this band is fragmented, feeding mainly into the positive parity ABCD and AB structures, as well as the ABCE negative parity band. Band DB1 in ^{196}Hg has similar excitation energy and spin, and it exhibits a similar decay pattern. No structure similar to DB2 is found in ^{194}Hg . In ^{192}Hg Le Coz et al [17] report two dipole bands. The first extends up to spin 34 from a bandhead spin of $23^{(-)}$ at 6879 keV, and decays mainly to the negative parity ABCE band, as is the case for

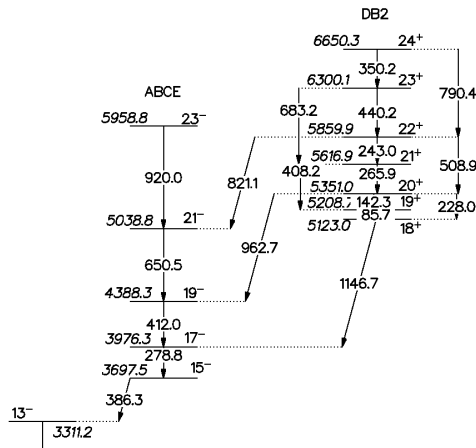


Figure 7. A partial level scheme of ^{196}Hg indicating the new dipole band DB2 as obtained from the present study.

DB2 in ^{196}Hg . However, it has opposite parity, and a higher excitation energy and bandhead spin. The second dipole band in ^{192}Hg has positive parity but decays to the positive parity AB band with no link to the negative parity bands. The bandhead spin is also higher than that of DB2.

There is thus no clear correspondence between DB2 in ^{196}Hg and any dipole band in the lighter even Hg isotopes. Further analysis is in progress in order to assign a configuration to this band.

Acknowledgments

This work is partly supported by the DFG, Germany, under grants SFB 634, NE 679/2-2 and SUA-111/3/04 as well as the NRF of South Africa.

References

1. M. Dasgupta, D. J. Hinde, N. Rowley, and A. M. Stefanini, *Ann. Rev. Nucl. Part. Sci* **48**, 401 (1998).
2. N. Rowley, G. R. Satchler, and P. H. Stelson, *Phys. Lett. B* **254**, 25 (1991).
3. H. Timmers *et al.*, *Nucl. Phys. A* **584**, 190 (1995).
4. S.S. Ntshangase *et al.*, *Phys. Lett. B* **651**, 27 (2007).
5. C. Fransen *et al.*, *Phys. Rev. C* **67**, 024307 (2003).
6. A. Shevchenko *et al.*, *Phys. Rev. Lett.* **93**, 122501 (2004).
7. H. Fujita *et al.*, *Nucl. Inst. and Meth. A* **483**, 17 (2002).
8. H. Fujita *et al.*, *Nucl. Phys. A* **788**, 94c (2007).
9. F. Hofmann *et al.*, *Phys. Lett. B* **661**, 165 (2005).

10. P. D. Kuntz, code CHUCK3, unpublished.
11. C. Fransen *et al.*, *Phys. Rev. C* **71**, 054304 (2005).
12. N. LoIudice, and Ch. Stoyanov, *Phys. Rev. C* **73**, 037305 (2006).
13. B. Cederwall *et al.*, *Phys. Rev. C* **47**, R2443 (1993).
14. E. Gueorguieva *et al.*, *Eur. Phys. J. A* **20**, 47 (2003).
15. D. Mehta *et al.*, *Z. Phys. A* **339**, 317 (1991).
16. N. Fotiades *et al.*, *Z. Phys. A* **354**, 169 (1996).
17. Y. Le Coz *et al.*, *Z. Phys. A* **348**, 87 (1994).